

Active Flow Control with DBD Plasma Vortex Generators around a NACA 2415 Airfoil

Hürrem Akbıyık¹, Hakan Yavuz²

¹ Çukurova Üniversitesi Mühendislik Fakültesi Makine Mühendisliği, ADANA

² Çukurova Üniversitesi Mühendislik Fakültesi Makine Mühendisliği, ADANA

(Alınış / Received: 26.03.2021, Kabul / Accepted: 28.08.2021, Online Yayınlanma / Published Online: 31.08.2021)

Keywords

Lift Coefficient,
Plasma Actuators,
Vortex Generators,
Pressure Coefficient,
Drag Coefficient

Abstract: In this study, the effect of dielectric barrier discharge vortex generator plasma actuators on pressure coefficients of a NACA2415 airfoil are investigated experimentally at a Reynolds number of 5×10^4 . The dielectric barrier discharge plasma vortex generators are placed at the leading edge of the airfoil. Force measurements with a six-axis load cell and free stream velocity with a pitot static tube are conducted. The pressure distributions over the airfoil are measured using a scan-valve unit and a pressure transducer. The experimental results showed that when the dielectric barrier discharge vortex generators were driven at a specific electrical parameter, the lift coefficient of the airfoil is increased significantly and the stall angle was postponed by induced flow effect. Moreover, the co-rotating dielectric barrier discharge vortex generators type is more effective than the counter-rotating type in reducing the drag coefficient. Furthermore, the 3D flow structure for both types of vortex generators was observed at the surface of the airfoil by using pressure measurements along with spanwise direction. In addition, it appears that the effect is less in the case of the stall angle in both plasma actuated state for drag coefficient, but they are more effective in the pre-stall angle and post-stall cases.

NACA2415 Kanat Modeli Etrafındaki Akışın DBD Plazma Girdap Üreteçleri ile Kontrolü

Anahtar Kelimeler

Kaldırma Katsayısı,
Plazma Aktüatör,
Girdap Üretici,
Basınç Katsayısı,
Sürüklenme Katsayısı

Öz: Bu çalışmada, girdap üretici olarak dielektrik bariyer deşarj plazma eyleyicilerinin NACA2415 kanat modelinin aerodinamik performansına etkileri basınç katsayısı göz önüne alınarak deneysel olarak Reynolds sayısının 5×10^4 olduğu değerde incelenmiştir. Dielektrik bariyer deşarj plazma girdap üreteçleri kanat modelinin ön kısmına yerleştirilmiştir. Kuvvet ölçümleri altı eksenli yük hücresi kullanılarak yapılmıştır ve serbest akış hızı pitot statik tüpü ile ölçülmüştür. Kanat modeli etrafındaki basınç dağılımları basınç dönüştürücü ve dairesel tarama vanası kullanılarak ölçülmüştür. Deneysel sonuçlar, dielektrik bariyer deşarj girdap üreteçleri belirli elektriksel parametrelerde sürüldüğünde kaldırma katsayısını önemli ölçüde arttırdığı ve stol açısını indirgenmiş akış etkisiyle geciktirdiğini göstermiştir. Dahası, eş dönümlü dielektrik bariyer deşarj girdap üreteçlerinin sürüklemeyi katsayısını azaltmada zıt dönümlü dielektrik bariyer deşarj tipine göre daha etkili olduğu gözlemlenmiştir. Ayrıca, kanat yüzeyinde üç boyutlu akış yapısı kanat açıklığı yönünde alınan basınç ölçümleri sayesinde her iki girdap üretici tarafından da oluşturulduğu ortaya gözlemlenmiştir. İlave olarak, her iki plazma girdap üreteçlerinin de sürüklenme katsayısı üzerine etkileri stol açısında daha az iken stol öncesi ve sonrası durumlarda daha fazla etkiye sahip olduğu gözlemlenmiştir.

*Corresponding Author, email: hakbiyik@cu.edu.tr

1. Introduction

In recent years, dielectric barrier discharge plasma actuators have been a popular topic for many researchers in aerodynamic applications due to their features such as simple structure, fast response time, having no moving parts and so on. In the aerodynamic field, they have critical applications such as plasma gurney flap[1,2], plasma travelling wave device[3,4], plasma tip-clearance seals[5] and plasma vortex generators[6-8]. The conventional mechanical vortex generators have a drag penalty. However, DBD plasma vortex generators can be activated on demand at required conditions. Due to their electrical structure, they can be adapted easily to the electrical system

of an aircraft. Choi et al. [9] reported that plasma virtual actuators can be used instead of conventional actuators. Akbilyk et al. [10] stated the effect of vertically placed plasma actuators on the lift and drag coefficient of an airfoil.

In the numerical and experimental study by Aram et al. [11], sDBD plasma actuators were used to control turbulent boundary layer separation. They reported that the Reynolds number for the study was set at 240000. In the plasma release signal, which is one of the critical parameters examined in the study, they compared the type of signal activated in a certain range (duty cycle) with sine wave. They revealed that the input signal has an important role in the efficiency of the plasma, beyond the plasma release voltage, in the development of the aerodynamic performance of the aircraft wing. Khoshkhoo and Jahangirian [12] conducted a study examining the activity time of plasma as another numerical study. In their studies, they examined plasma actuators placed on the NACA0015 aircraft wing model as key parameters in the flow separation control as a result of continuous triggering at regular intervals. They revealed that the body force created with the help of plasma enables the flow to hold on to the wing and it affects the boundary layer development. Sun et al. [13] stated in their study that plasma actuators triggered at certain intervals, that is, the momentum transfer in the opposite direction due to the effects of the gaps formed during the release, was prevented. Zhang et al. [14] experimentally investigated the turbulence boundary layer separations using symmetrical plasma actuators at high Reynolds number in their study. In their experimental studies, they revealed that the wing significantly suppresses the turbulence boundary layer separations with the help of plasma actuators. In addition, they achieved a maximum improvement of 9% in lift force and shifted the stall angle by 2 degrees. These actuators have been successfully used to form the flow around bodies [15] and used in boundary layers [16,17]. Most of the plasma actuators are placed along the spanwise direction in order to generate induced flow and to add momentum to the flow in the literature. However, two rows of DBD plasma actuators were used in a turbulent boundary layer so as to produce a spanwise force [18,19]. When the skin friction was reduced, the streamwise vortices were generated by the plasma actuators. Okita et al. [20] used a yawed DBD plasma actuator by generating a large-scale streamwise vortex that delay flow separation around a NACA2415 airfoil. Porter et al. [21] and Bolitho and Jakob [22] reported the tangential jets by using two opposing plasma actuators. They showed that varying the produced induced flow can be vectored to generate a jet that is similar to a vortex generator.

Recent studies about the vortex generator application as passive and active flow control devices is given in the following sentences. Hu et al. [23] investigated the effects of DBD vortex generator (DBD-VG) on flow around the Ahmed body that is vehicle model. DBD-VG actuators placed to back slope of the Ahmet body model. Their results indicates that DBD-VG provides 8.51% drag reduction with the driving voltage of 13kV. Vernet et al. [24] performed the experimental study by using DBD-VG for truck-trailer model. Their results showed that DBD-VG provides a drag reduction of 20%. They placed the actuators at the leeward sides which is located in front of the truck. Natarajan et al. [25] studied the influence of bio-inspired bristled shark skin vortex generator on the submarine model. Said et al. [26] performed the experimental study to research the optimum location of micro vortex generator on flow around the NACA 4415 airfoil. They found the optimum position to be chord length of 30%. As seen in the studies given above, these vortex generators are still widely used in the literature for both active and passive flow control applications. In this study, the co-rotating and counter-rotating plasma vortex generators and their contribution to aerodynamic performance of a NACA2415 airfoil has been studied. Moreover, the aim of this study is to show the potential of yawed plasma actuators in flow control applications. Pressure coefficient of the airfoil is measured in spanwise and in chordwise directions in order to present the three-dimensional effects of plasma vortex generators. By using smoke-wire flow visualization technique, the flow around the airfoil is also examined prominently.

2. Material and Method

Experiments were conducted in an open-suction type wind tunnel with plexiglass test section of $1000\text{mm} \times 570\text{mm} \times 570\text{mm}$. The NACA2415 airfoil was used as a test model and the DBD VGs plasma actuators placed at the leading edge of this airfoil as it seen in Figure 1. The chord length and spanwise length of the airfoil are 150 mm and 500 mm, respectively. The 280mm end plates located at both top and bottom sides of the test section.

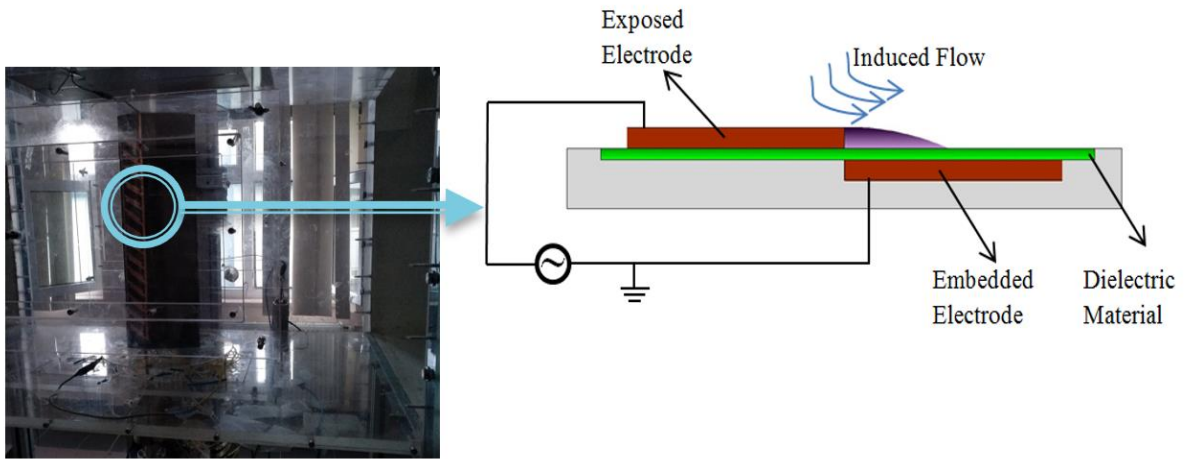


Figure 1. The test model in wind tunnel and structure of the plasma actuator

As it is seen in Figure 2, two different electrode geometry configurations namely as co-rotating and counter-rotating types plasma actuators are used to control of flow around airfoil.

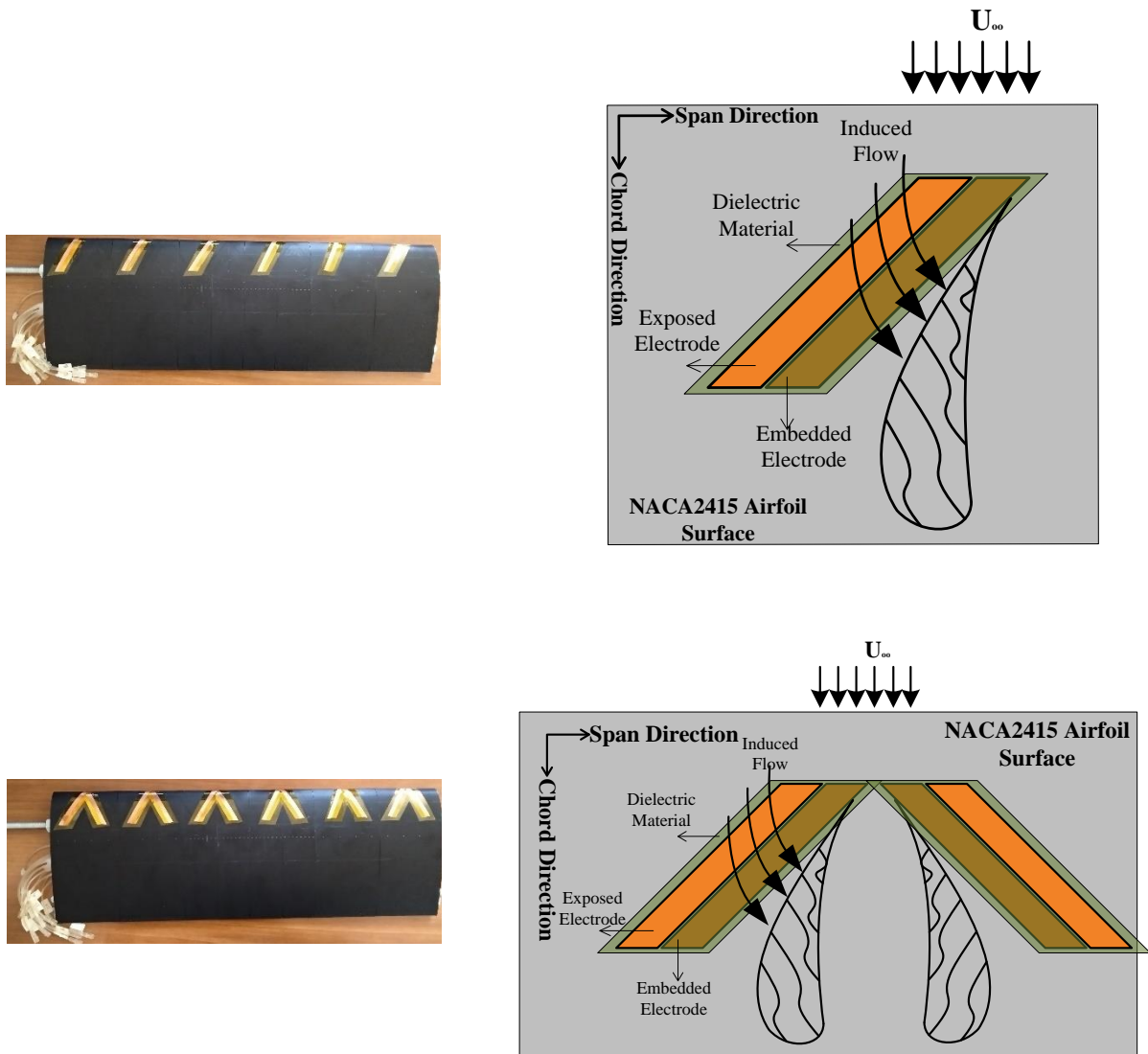


Figure 2. Structures of the co-rotating and counter-rotating plasma vortex generators

The dielectric barrier discharge vortex generators (DBD VGs) placed on the surface of the airfoil at $x/C = 0.1$ where "x and C" denotes direction and chord length, respectively. Each plasma actuator includes an embedded and an exposed electrode. Kapton is the dielectric material with thicknesses of 0.07 mm and it is placed between

embedded and exposed electrodes. A DBD VGs generates an induced flow which is perpendicular to the free stream flow. The structure of the accretive vortex depends on electrical properties of the plasma actuators such as applied voltage, excitation frequency, duty cycle, signal type; structures of actuators such as types of dielectric material, the thickness of dielectric material, length of the electrodes, width of the electrodes; flow properties such as types of fluid (Helium, Argon, Oxygen), free stream velocity; ambient conditions such as temperature, pressure and etc.; and the electrode placement angle to the surface of a model (yaw angle). In particular, the growth and decay of this vortex related to many of given parameters. The electrode lengths are carefully arranged as 50mm and yawing angles of the actuators are set to 45 degrees. In this study, the plasma generation system and electrical measurement devices are illustrated in Figure 3 and 4(b). In plasma generation, a custom-made amplifier is used to drive the plasma actuators. The plasma actuator driven parameters are set to 7 kV_{pp} applied voltage and 4 kHz excitation frequency. The signal type in this study is sinusoidal and monitored by Tektronix TDS2012B model oscilloscope. A Tektronix P6015A model voltage probe connected to this oscilloscope to measure the applied voltage.

Aerodynamic forces are measured by using an ATI Gamma model six axes load cell. Test model mounted on a rotary unit with a connection rod in order to set the attack angle of the model. The sampling frequency of the force measurement is 500 Hz and the experiments taken during the 10 second period. So, each measurement includes 10000 sampled values and repeated twice. Angle of attacks for the force measurement is varied between 0° and 16° with an increment of 2°. Uncertainty for the force measurement is calculated to be lower than 5%.



Figure 3. General view of the test setup

The pressure values acting over the NACA2415 airfoil surface were measured by using pressure taps. These pressure taps were located on the surface of the airfoil along the chord direction. The pressure taps were connected to a circular 36 channel scan-valve that transfers pressure values to a pressure transducer. The data taken from the pressure transducer were collected with the help of NI DAQ card. As it seen from Figure 4(a and c), the hose of the pressure transducer was connected to the coordinated pressure sockets on the wing, and measurements were taken. The other measurements were made from the tunnel test zone wall where the stream velocity is free stream type. The pressure coefficient distribution graph was obtained by dividing the difference of the pressure values taken from each pressure taps over the velocity values taken from the pitot tube used in the tunnel.

$$C_p = \frac{P_2 - P_1}{\frac{1}{2} \rho U^2} \quad (1)$$

The pressure coefficients were calculated by using Equation 1, where, U is the free stream velocity, P₂ and P₁ are the values read for each station from the pressure transducer, and ρ is the density of the air. The results represent the underlying dynamics for each pressure station at 0, 4, 8, 10, 12 and 16 degrees of attack angles. Uncertainty for the pressure measurement is calculated to be lower than 3.7%. In order to observe the flow around the NACA 2415 airfoil, a smoke-wire flow visualization method is utilised. Liquid form paraffin is dropped down to the wire for producing of white smoke. A power supply is used to heat the wire. The flow structure around the NACA2415 airfoil is visualized with a camera.

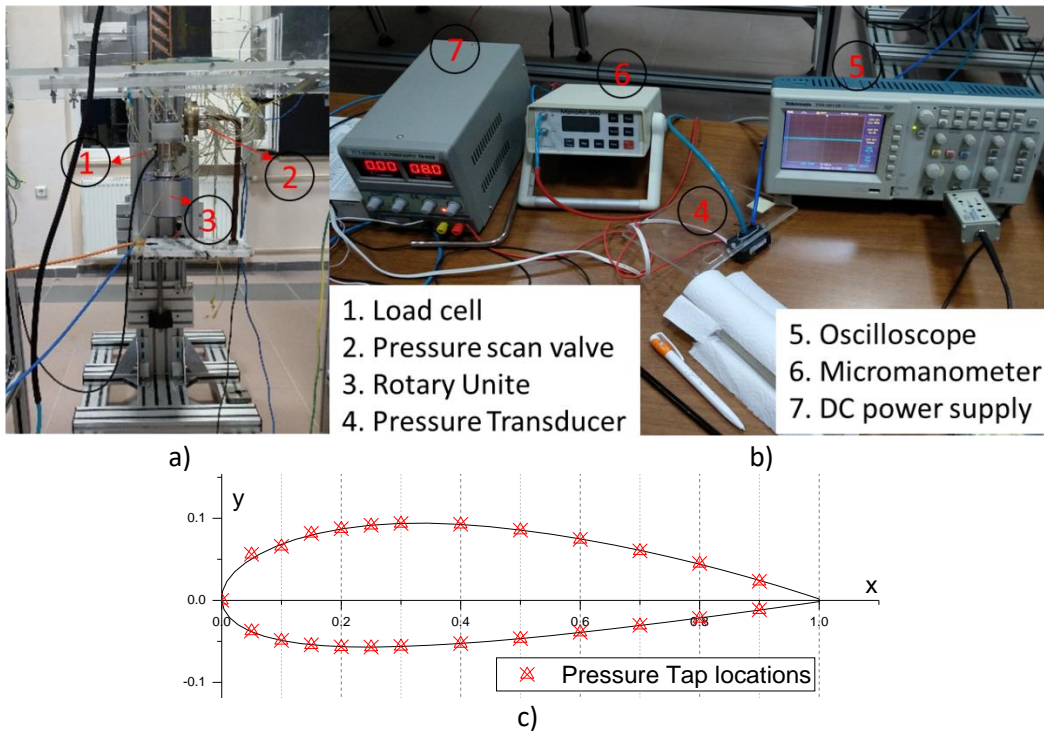


Figure 4. (a) force measurement system, (b) measurement devices and (c) schematic view of pressure tap locations

3. Results and Discussions

In this study, the effect of two different DBD-VGs plasma actuators placed on the NACA2415 aircraft wing along the span of the drag and lift force was investigated. The plasma applied voltage was set as 7 kV and frequency as 4 kHz, and the experiments are performed at $Re= 50000$. It is known that the range of Reynolds number defined is compatible with the flow conditions of MAVs and UAVs as it is reported by the study of Mueller[27]. In pressure coefficient measurements, the base model pressure coefficient was measured along chord for DBD-VGs Co and Counter Rotating models.

The aerodynamic coefficients such as lift (C_L) and drag (C_D) and lift to drag ratio (L/D) versus the angle of attack (AoA, α) for the NACA 2415 airfoil are presented in Figure 5(a-c). It is apparent that the lift coefficient increases with the increase of AoA. The C_L of the base NACA2415 airfoil increases linearly till 8 degrees with a maximum lift coefficient around 0.85. After 8 degrees of AoA, the lift coefficient of the airfoil decreases gradually because of the stall phenomenon. Considering the plot of the lift coefficient according to the angle of attack, it is observed that the lift coefficient of the base NACA2415 model is improved compared to the case for which the plasma actuators are used. It has been experimentally demonstrated that counter-rotating DBD-VGs type plasma actuators have a higher increase in lifting force compared to the case with co-rotating DBD-VGs plasma actuators. In addition, it was observed that the stall angle was shifted around 2 degrees compared to that of the base model for both plasma actuator cases. The stall angle was determined as 8 degrees for the base model, while it was observed as 10 degrees in the other case. It was observed that the lift coefficient of 0.85 at this angle value was increased to approximately 1.15 when the plasma was activated.

Also, the C_D of the NACA2415 airfoil increases with the increase of AoA. The C_D of the base NACA2415 airfoil increases slightly till 8 degrees. However, after the stall angle, the drag coefficient of the base airfoil increases gradually. When analyzed in terms of drag force, again, it is observed that both DBD-VGs plasma actuator cases drag coefficient is reduced compared to that of the base model NACA2415. However, it is clearly seen in the drag coefficient vs. AoA graph (in Figure 5(b)) that the DBD-VGs co-rotating plasma actuator structure is more effective than the counter-rotating model in reducing the drag coefficient. In addition, it appears that the effect is less in the case of the stall angle in both plasma actuated state, but they are more effective in the pre-stall angle and post-stall cases. Within the scope of this study, when the aerodynamic forces are analysed and interpreted together, the structures with plasma actuators are enabled to have a shorter take-off distance, also consume less fuel for the same journey, hence the running cost is reduced and the overall flight range is extended with improvements in aerodynamic design (C_L/C_D) (as shown in Figure 5(c)) for aircraft compared to the features of the base model. In addition, the experimental results of the study show that the presented active models play a critical role in reducing the drag coefficient. In special applications, the co-rotating DBD-VGs plasma actuated structure and the

counter rotating DBD-VGs plasma actuated structures have critical importance considering the improvements achieved in respective the lift coefficients.

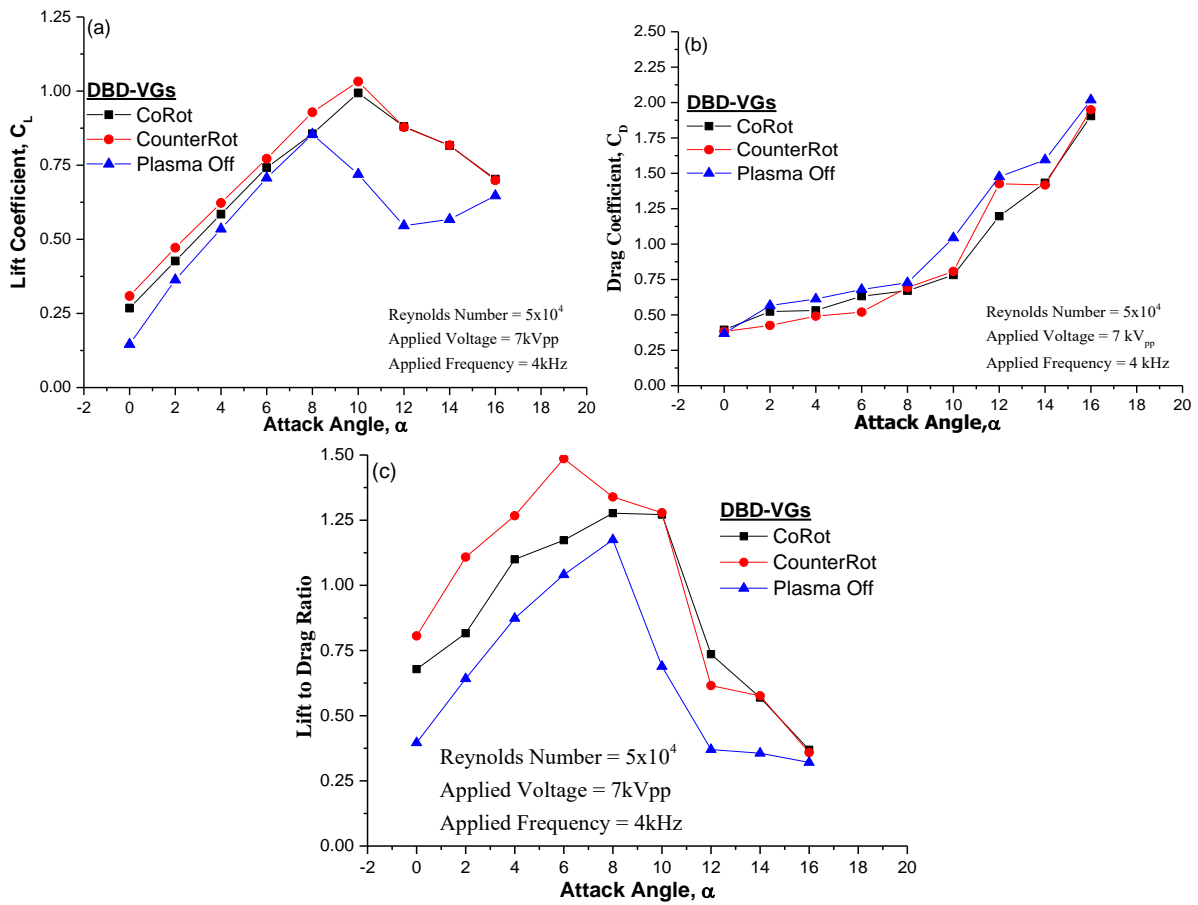


Figure 5. The effect of DBD-VGs Co- and Counter-rotating plasma actuator for (a) the lift coefficient, (b) drag coefficients and (c) lift to drag ratio of the NACA2415 airfoil

In Figure 6, the angle of attack of the NACA2415 wing model shows the pressure coefficients at different positions taken for various attack angles. Within the scope of this study, it is seen in the values in the graph that the pressure distributions for the basic model are uniform and they are compatible with the literature. The pressure difference between the suction and pressure surfaces of the basic model supports the lifting force acting on the wing model. When Laminar Separation Bubble (LSB) occur on the surface of the airfoil, it leads to changes on pressure coefficient of the airfoil. This LSB gives rise to significant increase in pressure coefficient after flow completes transition process. Then, the flow becomes more energetic and reattaches the surface of the airfoil. The LSB can be divided into two group as long and short bubbles [28]. Short bubbles may cause reattachment of the separated flow. Also, after the short bubble process, long bubbles may occur and this can be resulted in early stall for the airfoil. In Figure 6, the counter-rotating type DBD VGs has higher C_p values than the co-rotating type when AoA is 0° . Also, it appears that the co-rotating DBD VGs equipped airfoil has short bubble whilst the co-rotating DBD VGs equipped airfoil has long bubble. Two types of DBD VGs have the short bubble for AoA is 4° . However, the transition point of counter-rotating type DBD VGs has higher than co-rotating type. This can be interpreted that LSB structure occurred by the counter-rotating DBD VGs has bigger than co-rotating type. On the other hand, it is apparent that the LSB for the base airfoil case has long type bubble. So, the lift coefficient increased significantly but bubble type was changed. For the angle of attack is increased to 8° , the base airfoil has again long bubble generated. When the plasma vortex generators are activated, the separation point and reattachment point of the flow are the same for the both actuator types. However, actual pressure distribution with laminar separation bubble line has a slight difference. In the case of 10° AoA, the stall angle is shifted. Moreover, the lift coefficient significantly improved but both plasma VGs give rise to short bubble type. After this critical AoA, the airfoil may stall early due to the short bubble structure. For the AoA is 12° , the LSB structure is long bubble but just lift coefficient increased. There is no improvement of aerodynamic forces when AoA is 16° . This means that plasma actuators are not effective after 16° for the applied electrical parameters.

Active Flow Control with DBD Plasma Vortex Generators around a NACA 2415 Airfoil

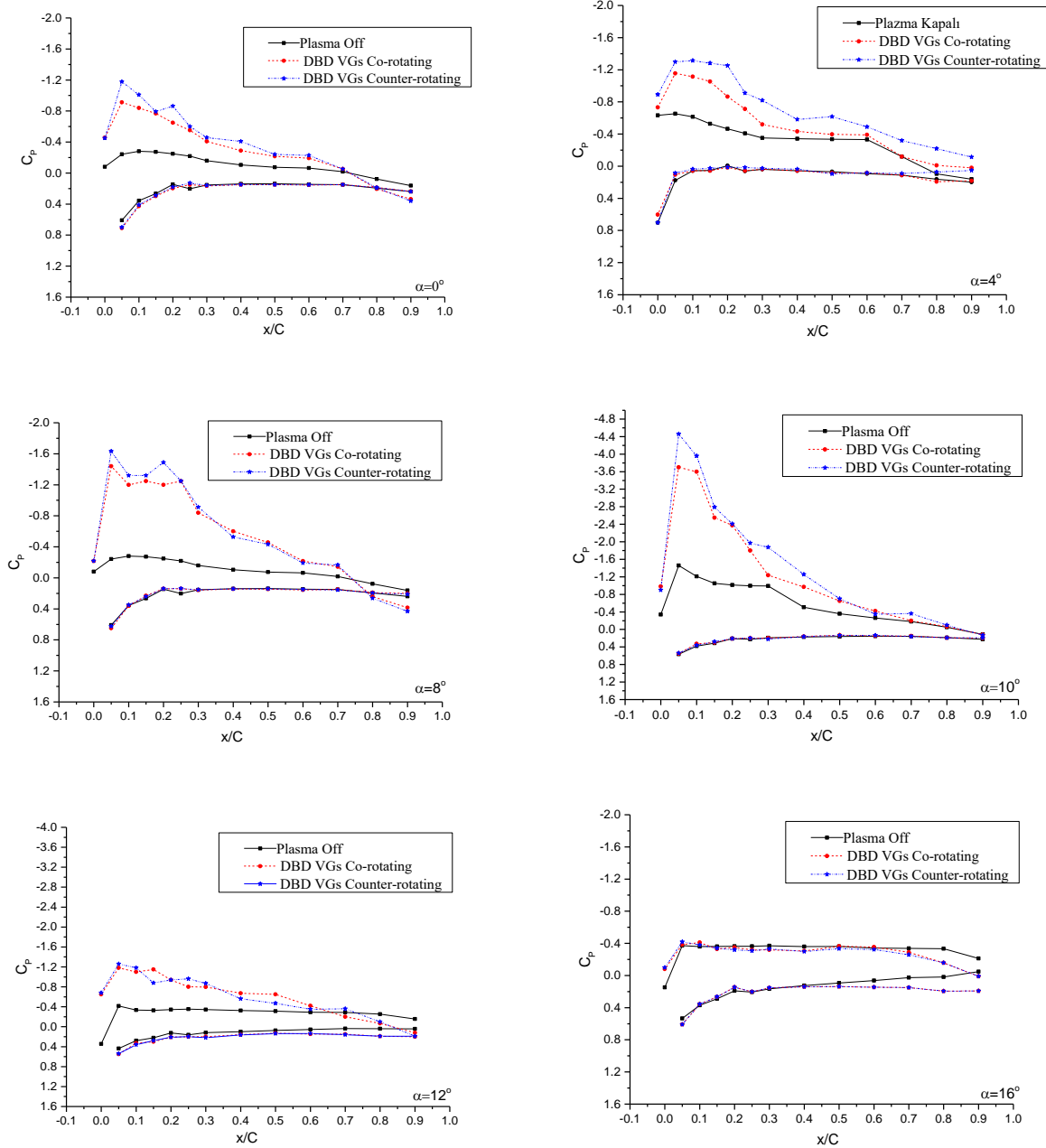


Figure 6. Chordwise pressure distribution of the NACA2415 airfoil at $Re = 5 \times 10^4$ and for varied attack angles

As seen in Figure 7, pressure coefficients of a NACA 2415 airfoil were measured for different attack angles where the pressure taps are placed at $x/C=0.4$ positions. The pressure taps are located this position in order to see the effects of plasma actuators. The pressure values taken from spanwise located pressure taps for the DBD VGs plasma actuators has 3D effects on the airfoil surface. As mentioned in Figure 2, The dielectric barrier discharge vortex generators located on the surface of the airfoil (with yaw angle) generated the induced flow that leads to initiate a process in which swirling flow occurred. The accretive longitudinal vortex changed the flow structure on the surface of the airfoil. In this case, the separated flow became close to the surface of the airfoil and increase the lift coefficient of the airfoil as well as the stall angle is shifted. Of course, the size of the accretive longitudinal vortex depends on some plasma generation parameters but especially related with yaw angle of actuators and length of the actuators. So, it appears that the change in 3D structure of generated vortex affects directly the aerodynamic properties of the airfoil. When the C_p values of the airfoil compared with the base airfoil in Figure 7, it can be said that both plasma actuators cases increase the lift coefficient. Furthermore, the fluctuating of C_p is an indication of 3D structure of flow generated by plasma vortex generators on the surface of the airfoil. It can be said that Counter-Rotating type vortex generators causes relatively more fluctuated flow on the surface of the airfoil due to adding more momentum to the flow. After the plasma vortex generators are activated, the pressure change, in the suction side of the airfoil, becomes clearly visible. The Counter-Rotating DBD VGs cause more changes in the pressure coefficient due to their structural features. The increase in the pressure difference between the suction and the

pressure side indicates that the lifting force is increased. Furthermore, the shifting in the stall angle and the increase in the lift force are clearly seen. It was observed that the measured pressure is increased due to the induced flow effect at the points where the plasma actuators were placed (x/C from 0.1 to 0.35). These plots show the details of the development of the boundary layer while the pressure increases after peak suction from LE to TE. Moreover, the distribution of pressure coefficient provides the details for the formation and progress the laminar separation bubble, transition and re-attached flow.

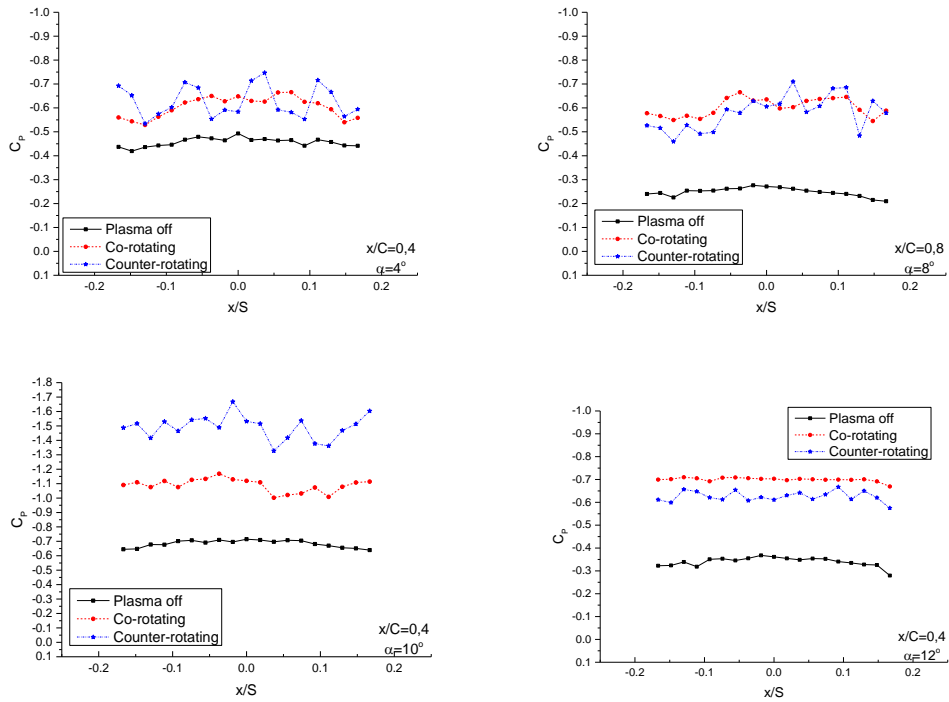


Figure 7. Spanwise pressure distribution of the NACA2415 airfoil at $Re = 5 \times 10^4$ and varied attack angles

The flow around the NACA2415 airfoil is visualized at 20×10^3 of Reynolds number. The flow structure around the airfoil is seen in Figure 8 at 10° of attack angle. Red dash line indicates the flow visualization plane for co-rotating and counter-rotating DBD-VG. For the plasma off case, it seems that the flow separated from the leading edge of the airfoil. But the separated flow comes near the surface of the airfoil when the plasma vortex generators are activated. It is seen that the flow visualization results support the pressure measurements and aerodynamic force measurements for the stall angle. It can be clearly reported that the plasma actuators have an important contribution to the flow control around the airfoil.

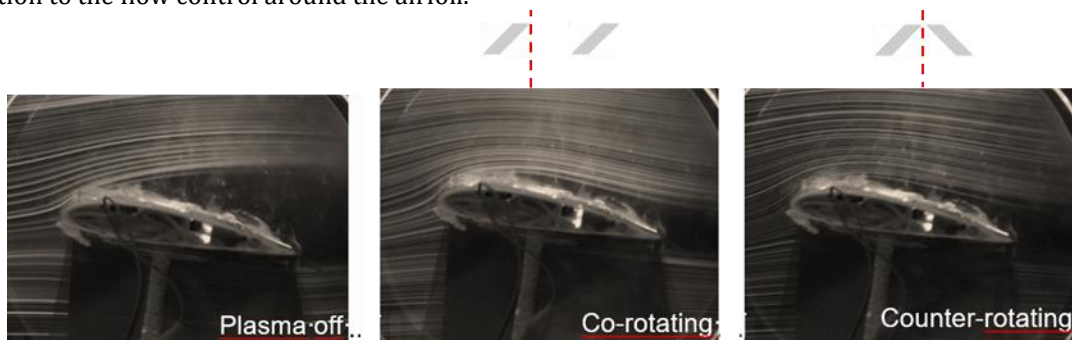


Figure 8. Flow visualization results for the base airfoil, co-rotating and counter-rotating DBD VGs airfoil at 10° of AoA

4. Conclusions

The main aim of this study is to gain some understanding of the phenomenon for the NACA2415 airfoil equipped with dielectric barrier discharge plasma vortex generators at low Reynolds number. The following list of conclusions achieved:

- The re-attached flow and laminar separation bubble formations are observed.
- Long and short bubble structures are experimentally investigated in this study.
- The 3D flow structure is generated by the DBD VGs plasma actuators and showed in the pressure coefficient results.
- The stall angle was shifted and the lift coefficient is increased.

- The drag coefficient of the airfoil is decreased for all cases. However, it is also observed that the decrease observed varies for different angle of attacks for both DBD-VGs models.

For further studies, varying effectiveness of electrical parameters of DBD-VGs plasma actuators and more vortex generator structures can be considered for an extended investigation. Moreover, the parameters that affect the structure of the accretive longitudinal vortex can be investigated in details such as electrical properties, structures of actuators, flow properties, ambient conditions and the electrode yawing angle. In addition, a sensor-actuator based control system can be implemented to the DBD-VGs vortex generators for aerodynamic flow control applications.

Acknowledgment

The authors would like to acknowledge the financial support of this work by the Scientific Research Projects (BAP) of the Çukurova University under the Contract Number of FBA-2019-12084.

Nomenclature

| | |
|----------------------|---|
| AoA | angle of attack |
| C | chord |
| CoRot | co-rotating |
| CounterRot | counter-rotating |
| C_D | drag coefficient |
| C_L | lift coefficient |
| C_P | pressure coefficient |
| DBD | dielectric barrier discharge |
| DBD-VG | dielectric barrier discharge vortex generator |
| LE | leading edge |
| LSB | laminar separation bubble |
| MAVs | micro air vehicles |
| sDBD | single dielectric barrier discharge |
| P | pressure |
| TE | trailing edge |
| Re | Reynolds number |
| U | free stream velocity |
| UAVs | unmanned air vehicles |
| VG | vortex generator |
| V_{PP} | peak to peak voltage |
| <i>Greek letters</i> | |
| α | angle of attack |
| ρ | density of the air |
| μ | dynamic viscosity of the air |
| x | direction |

References

- [1] Wang, J. J., Li, Y. C., Choi, K. S. 2008. Gurney Flap-Lift Enhancement, Mechanisms and Applications. *Progress in Aerospace Sciences*, 44, 22-47.
- [2] Zhang, P. F., Liu, A. B., Wang, J. J. 2009. Aerodynamic Modification of a NACA 0012 Airfoil by Trailing-Edge Plasma Gurney Flap. *AIAA Journal*, 47, 2467-2474.
- [3] Zhao, H., Wu, J. Z., Luo, J. S. 2004. Turbulent Drag Reduction by Traveling Wave of Flexible Wall. *Fluid Dynamics Research*, 34, 175-198.
- [4] Itoh, M., Tamano, S. 2012. Drag Reduction in Turbulent Boundary Layers by Spanwise Travelling Waves with Wall Deformation, *Journal of Turbulence*, 13, 1-26.
- [5] Saddoughi, S., Bennett, G., Boespflug, M., Puterbaugh, S. L., Wadia, A. R. 2015. Experimental Investigation of Tip Clearance Flow in a Transonic Compressor with and without Plasma Actuators. *Journal of Turbomachinery*, 137, 1-10.
- [6] Jukes, T., Choi, K. S. 2013. On the Formation of Streamwise Vortices by Plasma Vortex Generators. *Journal of Fluid Mechanics*, 733, 370-393.

- [7] Jukes, T., Choi, K. S. 2012. Dielectric-Barrier-Discharge Vortex Generators: Characterization and Optimization for Flow Separation Control. *Experiments in Fluids*, 52, 329-345.
- [8] Segawa T., Furutani H. 2013. Flow Control on a NACA 4418 Using Dielectric-Barrier-Discharge Vortex Generators. *AIAA Journal*, 51, 452-464.
- [9] Choi, K. S., Jukes, T. N., Whalley, R. D., Feng, L. H., Wang, J. J., Matsunuma, T., Segawa, T. 2015. Plasma Virtual Actuators for Flow Control. *Journal of Flow Control, Measurement & Visualization*, 3, 22-34.
- [10] Akbıyık, H., Yavuz, H., Akansu, Y. E. 2016. Investigation of the Effect of the Plasma Actuators Vertically Placed on the Spanwise of NACA0015 Airfoil. 8th International Exergy, Energy and Environment Symposium (IEEES-8), 1-4 May, Antalya, Turkey.
- [11] Aram, S., Shan, H., Lee, Y. T. 2016. Application of an Integrated Flow and Plasma Actuation Model to an Airfoil. *AIAA Journal*, 54, 2201-2210.
- [12] Khoshkhoo, R., Jahangirian, A. 2016. Numerical Simulation of Stall Flow Control Using a DBD Plasma Actuator in Pulse Mode. *Plasma Science and Technology*, 18, 933-942.
- [13] Sun, M., Yang, B., Peng, T., Lei, M. 2016. Optimum Duty Cycle of Unsteady Plasma Aerodynamic Actuation for NACA0015 Airfoil Stall Separation Control. *Plasma Science and Technology*, 18, 680-685.
- [14] Zhang, X., Huang, Y., Wang, X., Wang, W., Tang, K., Li, H. 2016. Turbulent Boundary Layer Separation Control Using Plasma Actuator at Reynolds Number 2000000. *Chinese Journal of Aeronautics*, 29, 1237-1246.
- [15] Jukes, T., Choi, K. S. 2009. Flow Control around a Circular Cylinder Using Pulsed Dielectric Barrier Discharge Surface Plasma. *Physics of Fluids*, 21, 1-12.
- [16] Moreau, E. 2007. Airflow Control by Non-thermal Plasma Actuators. *Journal of Physics D: Applied Physics*, 40, 605-636.
- [17] Grundmann, S., Tropea, C. 2008. Active Cancellation of Artificially Introduced Tollmien-Schlichting Waves Using Plasma Actuators. *Experiments in Fluids* 44, 795-806.
- [18] Jukes, T., Choi, K. S., Johnson, G., Scott, S. 2006. Turbulent Drag Reduction by Surface Plasma Through Spanwise Flow Oscillation. In: 3rd AIAA Flow Control Conference, 5-8 June, California, USA.
- [19] Choi, K. S., Jukes, T., Whalley, R., 2011. Turbulent Boundary-Layer Control with Plasma Actuators. *Philosophical Transactions of the Royal Society A*, 369, 1443-1458.
- [20] Okita, Y., Jukes, T., Choi, K. S., Nakamura, K. 2008. Flow Reattachment over an Airfoil Using Surface Plasma Actuator. 4th AIAA Flow Control Conference, 23-26 June, Washington, USA.
- [21] Porter, C., Abbas, A., Cohen, K., McLaughlin, T., Enloe, C. L. 2009 Spatially Distributed Forcing and Jet Vectoring with a Plasma Actuator. *AIAA Journal*, 47, 1368-1378.
- [22] Bolitho, M., Jacob, J. 2008. Thrust Vectoring Flow Control Using Plasma Synthetic Jet Actuators. 46th AIAA Aerospace Sciences Meeting and Exhibit, 7-10 January, Nevada, USA.
- [23] Hu, X., Zhang, J., Hui, Z., Luo, Y., Guo, P., & Wang, J. 2021. Flow control of automobile with plasma vortex generator. *Journal of Mechanical Science and Technology*, 35(6), 2493-2502.
- [24] Natarajan, E., Freitas, L. I., Chang, G. R., Al-Talib, A. A. M., Hassan, C. S., & Ramesh, S. 2021. The hydrodynamic behaviour of biologically inspired bristled shark skin vortex generator in submarine. *Materials Today: Proceedings*, 46, 016009.
- [25] Vernet, J. A., Örlü, R., Söderblom, D., Elofsson, P., & Alfredsson, P. H. 2018. Plasma streamwise vortex generators for flow separation control on trucks. *Flow, turbulence and combustion*, 100(4), 1101-1109.
- [26] Said, I., Poonasparan, M. K., Bohari, B., Idris, A. C., Rahman, M. R. A., & Saad, M. R. 2021. The Effect of Streamwise Location of Micro Vortex Generator on Airfoil Aerodynamic Performance in Subsonic Flow. *Journal of Aeronautics, Astronautics and Aviation*, 53(2), 173-178.
- [27] Mueller, T. J. 1999. Aerodynamic Measurements at Low Reynolds Numbers for Fixed Wing Micro-Air Vehicles. Development and Operation of UAVs for Military and Civil Applications, Hessert Center for Aerospace Research, University of Notre Dame, 8.1-8.32.
- [28] Horton, H. P. 1968. Laminar Separation Bubbles in Two and Three Dimensional Incompressible Flow, University of London, UK.